RSC Advances

PAPER

View Article Online
View Journal | View Issue

Cite this: *RSC Adv.*, 2020, **10**, 42706

Unraveling the mechanism of CO_2 capture and separation by porous liquids†

Jie Yin,[a] Wendi Fu,[a] Jinrui Zhang,[a] Hongshun Ran,[a] Naixia Lv,[b] Yanhong Chao,[a] Hongping Li,*[a] Wenshuai Zhu,*[a] Hui Liu*[a] and Huaming Li[a]

Carbon dioxide (CO_2) emissions intensify the greenhouse effect so much that its capture and separation are needed. Porous liquids, possessing both the porous properties of solids and the fluidity of liquids, exhibit a wide range of applications in absorbing CO_2, but the mechanism of gas capture and separation demands in-depth understanding. To this end, we provide a molecular perspective of gas absorption in a porous liquid composed of porous organic cages dissolved in a size-excluded solvent, hexachloropropene, by density functional theory for the first time. In this work, different conformations were considered comprehensively for three representative porous organic cages and molecules. Results show that chloroform, compared to CO_2, tends to enter the cage due to stronger C–H···π interaction and the optimal capacity of each cage to absorb CO_2 through hydrogen bonding and π–π interaction is 4, 2 and 4 equivalents, respectively. We hope that these discoveries will promote the synthesis of similar porous liquids that are used to capture and separate gases.

Received 20th September 2020
Accepted 16th November 2020

DOI: 10.1039/d0ra08039j

rsc.li/rsc-advances

1. Introduction

With the increase of carbon dioxide emissions from fossil fuels, human health and the living environment have been seriously threatened due to the intensification of the greenhouse effect. Therefore, carbon dioxide capture and separation are particularly significant. Currently, the capture of CO_2 includes not only solid adsorption, such as with metal organic frameworks (MOFs)[1–3] and zeolites,[4–6] but also liquid absorption, especially with ionic liquids.[7–12]

As a new type of material, porous liquids have been a research hotspot since James *et al.*[13] proposed the concept in 2007. In general, porous liquids are divided into three categories. One is pure substances with permanent pores, and the other two are those that dissolve rigid porous materials in sterically hindered solvents.[13] It is the porous liquid that not only possesses the cavity of the porous material, but also combines the fluidity of the liquid, thus it has a huge application prospect in the storage and transportation of gas.

However, the difficulty of preparation greatly limits the development of porous liquids, resulting in a few related reports,[14–24] many of which are more about porous organic cages.[25] Jie *et al.*[15] successfully developed a porous liquid based on an anionic organic covalent cage and crown ether through a supramolecular complexation strategy. James *et al.*[22] modified the vertices of porous organic cages (POCs) with alkyl groups to make type I porous liquid. After that, a type II porous liquid containing crown ether modified POCs, dissolved in the size-excluded solvent 15-crown-5, is proposed.[17] Owing to the high viscosity of the crown ether type porous liquid, the complicated production process and the low yield, a simple preparation type II porous liquid was introduced. The porous liquid consists of POCs formed by substituting amines in sterically hindered solvent hexachloropropene (PCP).[17] These two liquids have a high absorption capacity for carbon dioxide, and it was found that after adding chloroform ($CHCl_3$), the absorbed carbon dioxide would be displaced. Now that porous liquids are a promising new class of materials for gas capture, it is necessary for us to further gain insight into these systems from a molecular perspective to design better performance materials easily. Hence, several issues deserve further study that types of the interaction, gas absorption capacity of the cage cavity and the replaced mechanism. Here, the interaction between CO_2 and the porous liquids as well as the displaced process needs more deep understanding at molecular level. In 2016, Zhang *et al.*[26] studied the thermodynamics and kinetics for the storage of CH_4, CO_2, and N_2 molecules in porous liquids by molecular dynamics (MD) simulations, which provided a dynamic view. By contrast, a static angle to systematically study the issues mentioned above is carried out through density functional theory (DFT) that is a method of studying the electronic structure of multi-electron systems and have encountered a wide range of applications to study molecular properties.[27,28]

[a]*Institute for Energy Research, School of Chemistry and Chemical Engineering, Jiangsu University, Zhenjiang, 212013, P. R. China. E-mail: hongpingli@ujs.edu.cn; zhuws@ujs.edu.cn; lh7544@ujs.edu.cn*

[b]*College of Biology and Chemistry, Xingyi Normal University for Nationalities, Xingyi, 562400, P. R. China*

† Electronic supplementary information (ESI) available. See DOI: 10.1039/d0ra08039j

In current work, we studied the optimal adsorption capacity of the cages and the interaction nature between POCs, CO_2, and $CHCl_3$ to elucidate the physics behind these macroscale characteristics from the microscopic point of view. Moreover, the exchange mechanism between chloroform and carbon dioxide is the dominated research content. After three representative POCs were properly constructed, various conformations where CO_2 or $CHCl_3$ lied in the cavity of the cage were considered in detail according to the symmetry of the cages. The results show that POCs have a certain adsorption capacity for CO_2, and the cage does provide a cavity for absorbing or containing CO_2. Furthermore, chloroform tends to interact with cavities more likely than CO_2, as a result, CO_2 will indeed be squeezed out by chloroform. It is hoped that this work will help to improve the absorption of CO_2 and the synthesis of POCs.

2. Computational details

2.1 Theory

Whether it is liquid absorption or solid adsorption, almost all non-covalent forces exist in the system.[7,29,30] Intermolecular non-covalent interactions, including hydrogen bonds, π–π interactions, C–H···π interactions, *etc.*, are the foundation and core content of supramolecular chemistry. In this work, there are also non-covalent forces between the porous organic cage and CO_2 (and/or $CHCl_3$). Related literature shows that the M0X-type density functional (*e.g.* M06-2X) of the Minnesota family with dispersion correction is widely used in such non-covalent systems.[27,28,31,32] Therefore, the M06-2X density function with dispersion correction in the Gaussian16 program[33] was selected as the method. In addition, considering the reasonableness of the calculation time and the accuracy of the results, the smaller basis set 6-31G (d) was first used for structural optimization, and then the larger basis set 6-311G (d,p) was employed to calculate the energy and physical properties.

2.2 Model

As a type II porous liquid, it is composed of hexachloropropene and porous organic cages (POCs). James *et al.*[17] proved that the cavity provided by POCs does provide a great contribution to gas absorption. In view of this, we selected a single POC as the research object. As shown in Fig. 1 and 2, each POC has four surfaces and windows, as well as six vertices. The **TFB** (1,3,5-tricarbonylbenzene) in blue forms the surface of the cage, and the "**3**" (1,2-cyclohexanediamine) in green as well as the "**13**" (1,2-diamino-2-methylpropane) in red constitute the vertices of the cage. Obviously, POCs can be distinguished by different vertices. Given the rationality and complexity of the model, we chose three kinds of POC as

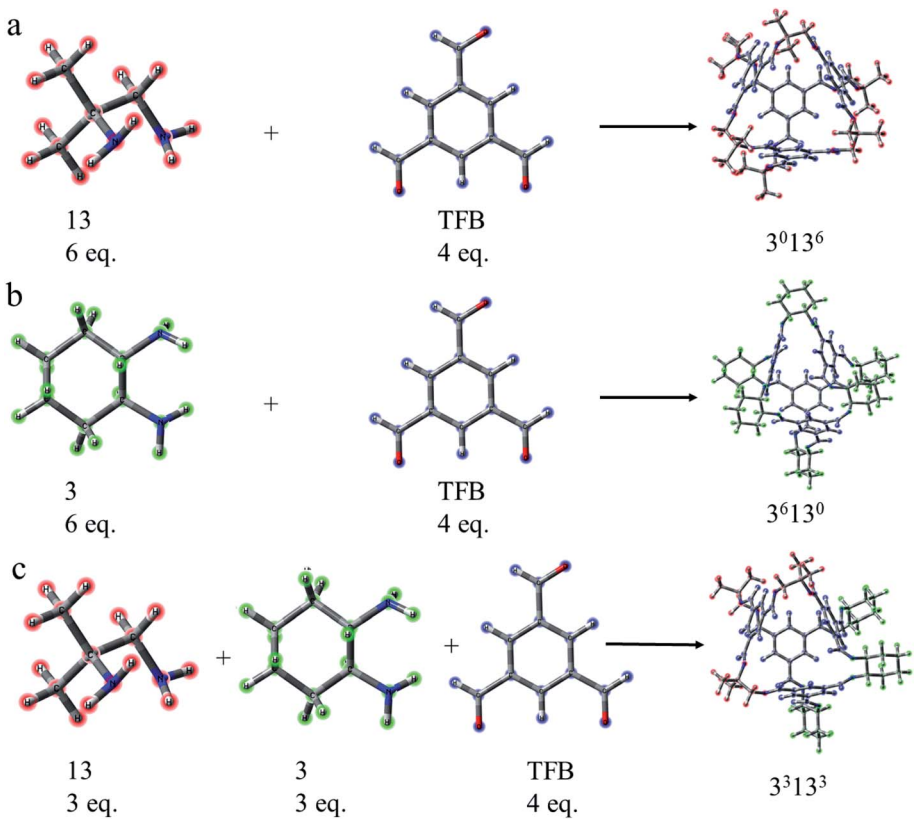

Fig. 1 Composition of porous organic cages. (a) Cage $3^0 13^6$. (b) Cage $3^6 13^0$. (c) Cage $3^3 13^3$. **TFB** (1,3,5-triformylbenzene) in blue constitutes the face of the cage while "**3**" (1,2-cyclohexanediamine) in green and "**13**" (1,2-diamino-2-methylpropane) in red form the vertex of the cage. $3^x 13^y$ represents the number of "**3**" (x) and the number of "**13**" (y) in each cage.

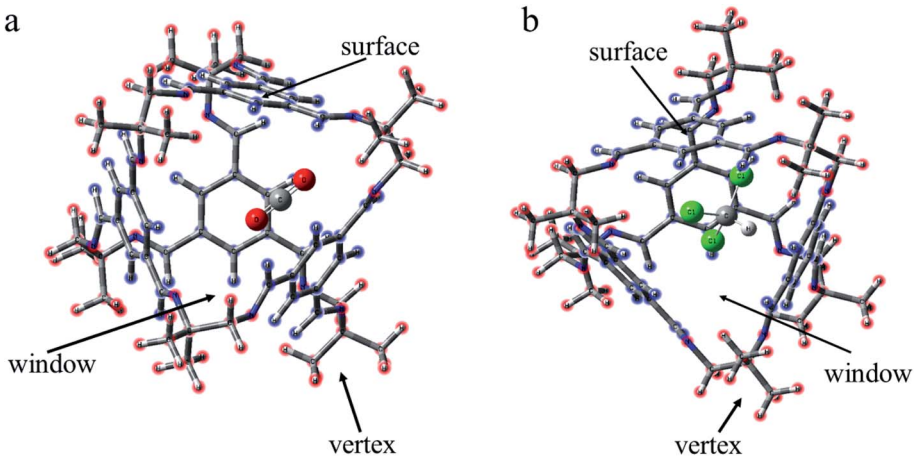

Fig. 2 Schematic of different conformations. (a) CO_2 lies inside the cage and $CHCl_3$ is at three locations outside the cage. (b) $CHCl_3$ lies inside the cage, and CO_2 stands at three locations outside the cage. Vertex means near the vertex formed by "**3**" ("**13**"). Window means in the hole of the cage. Surface means on the benzene ring of TFB.

representatives. $\mathbf{3}^x\mathbf{13}^y$ is defined as the number of 1,2-cyclohexanediamine (x) and the number of 1,2-diamino-2-methylpropane (y) in each cage. Thus, the three cages are named $\mathbf{3}^0\mathbf{13}^6$, $\mathbf{3}^6\mathbf{13}^0$ and $\mathbf{3}^3\mathbf{13}^3$ respectively. By investigating the different positions of CO_2 and $CHCl_3$, the mechanism of $CHCl_3$ displacing CO_2 was explored.

In order to intuitively understand the magnitude of the interaction between CO_2/$CHCl_3$ and the cavity, the interaction energy was calculated according to the following formula:

$$E_{abs} = E_{opt} - E_{cage} - E_{CO_2} - E_{CHCl_3} + E_{BSSE} \quad (1)$$

Among them, E_{opt} is the optimized energy of placing CO_2 and $CHCl_3$ around the POC. E_{cage} is the energy of the cage. E_{CO_2} and E_{CHCl_3} represent the energy of carbon dioxide and chloroform, respectively. To obtain precise results, the basis set supper position error (BSSE) was taken into account. Generally speaking, the value of E_{abs} is negative. The greater its absolute value is, the stronger the force will be.

Furthermore, the exchange energy is defined to investigate the possibility for separation of CO_2, which was calculated as follows:

$$E_{exc} = E_{out} - E_{in} \quad (2)$$

Among them, E_{out} refers to the lowest energy of the conformation in which CO_2 stands outside the cage and $CHCl_3$ lies inside the cage. E_{in} is the lowest energy of the conformation where CO_2 lies inside the cage and $CHCl_3$ stands outside the cage. E_{exc} is the exchange energy of CO_2 and $CHCl_3$. The positive or negative value indicates the stability of the conformation. If it is a positive value, it means that CO_2 is relatively stable in the cage whereas a negative value indicates that $CHCl_3$ in the cage is more stable. Hence, a negative value shows the potential to separation of CO_2 after absorption.

What's more, in order to explore gas absorption capacity, the interaction energy of each gas molecule in per cage was obtained:

$$\Delta\bar{E}_{aver} = 1/n(E_{opt} - E_{cage} - nE_{CO_2} + E_{BSSE}) \quad (3)$$

Among them, n is the number of gases. E_{opt} is the energy after structure optimization. E_{cage} represents the energy of the cage. E_{CO_2} is the energy of a single CO_2. Certainly, the BSSE was also included.

3. Results and discussion

3.1 Structures

For the structural analysis, there may be π–π interaction between CO_2 and benzene ring, and C–H···π interaction, as well as Cl···π interaction, between chloroform and benzene ring. In order to clearly understand the magnitude of these forces, three model structures were separately construct as shown in Fig. S1.† We might as well take the center of the benzene ring as X, and then use the dashed line connecting the O atom above the benzene ring and X as the distance from CO_2 to the benzene ring. Similarly, the interaction distance of C–H···π is the dashed line connecting the H atom and X, and the distance of Cl···π is the dashed line connecting the Cl atom and X. Besides, the energy and distance of the above three structures are listed for reference. It can be seen that the value of C–H···π is greater than the other two forces. As is shown in Fig. 2, according to the symmetry of the POC, except for the cavity, we considered three sites, namely the vertex, the window and the surface, which represents near the vertex formed by "**3**" ("**13**"), in the hole of the cage and on the benzene ring of **TFB**, respectively. Then, the positions of the inner and outer molecules of the POC were exchanged to obtain three other conformations.

Cage $\mathbf{3}^0\mathbf{13}^6$. In Fig. 3, all possible forces are connected with dashed lines. The relevant parameters are listed in Table S1.† First of all, the three situations were shown where CO_2 lies inside the cage and $CHCl_3$ stands outside the cage (Fig. 3a–c). When CO_2 is in the cage, the CO_2 structures of the three conformations are not much different. Among them, there are only three benzene rings satisfying the condition of Fig. S1a.† However, the distance between CO_2 and the benzene ring in the

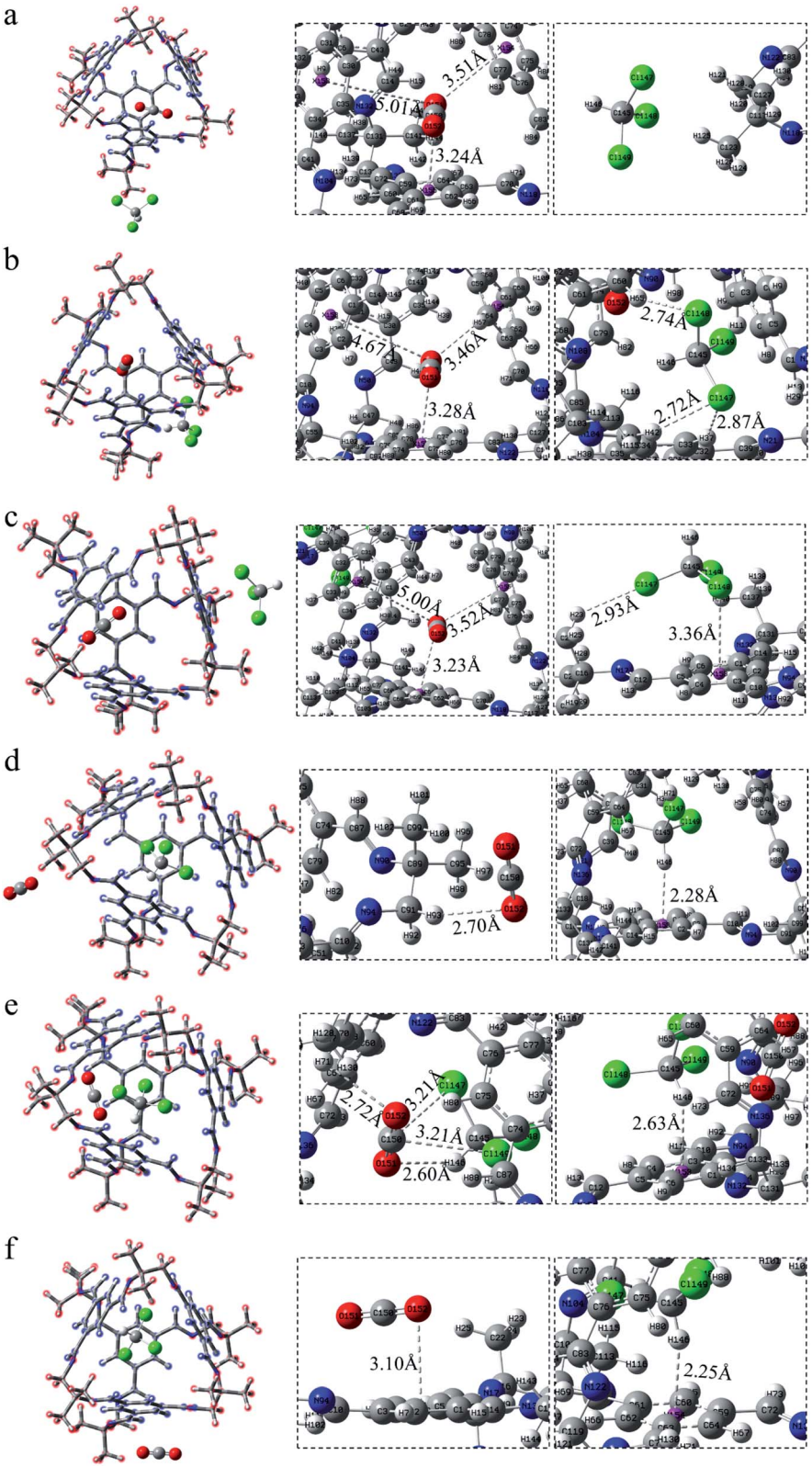

Fig. 3 CO_2 lies in the cage $3^0 13^6$ whereas $CHCl_3$ stands (a) COM-a, at the vertex; (b) COM-b, inside the window; (c) COM-c, on the surface. $CHCl_3$ lies in the cage $3^0 13^6$ whereas CO_2 stands (d) COM-d, at the vertex; (e) COM-e, inside the window; (f) COM-f, on the surface.

cage is farther than the model, so the force is not strong. In Fig. 3a, $CHCl_3$ has no hydrogen bond with the vertex. There are three hydrogen bonds between $CHCl_3$ and the cage window in Fig. 3b, which are Cl148⋯H65–C145 (2.74 Å), Cl147⋯H42–C145 (2.72 Å) and Cl147⋯H37–C145 (2.87 Å). When $CHCl_3$ is on the surface, the distance in Fig. 3c between the atom Cl148 and

the benzene ring is 3.36 Å, greater than that in Fig. S1c† (3.26 Å). What's more, chloroform has a weak hydrogen bond Cl147⋯H23–C145 (2.93 Å) with the vertex. Since the C–H⋯π between the C–H in $CHCl_3$ and the benzene ring has a strong force, we focus on the change of the C–H bond length. The C–H of the above three structures (Fig. 3a–c) has no force within the van der Waals radius. However, according to Table 1, the C–H bond length in Fig. 3b is elongated to 1.092 Å. This is because there are several hydrogen bonds in $CHCl_3$, and its own charge distribution may change, thereby affecting the bond length.

After exchanging the molecules in the cavity of the POC, $CHCl_3$ lies in the cage (Fig. 3d–f). The main force between $CHCl_3$ and the cavity is C–H⋯π. The shortest interaction distance is in Fig. 3f (2.25 Å) while the longest is in Fig. 3e (2.63 Å). The distance between C–H⋯π in Fig. 3d and f is close to that in Fig. S1b,† indicating that the force may be stronger. In Fig. 3d, CO_2 has a weak hydrogen bond with the vertex O152⋯H93–C91 (2.70 Å). Also, there is a hydrogen bond O152⋯H71–C70 (2.72 Å) at the window between CO_2 and the cage in COM-e. It is worth noting that there remain forces between CO_2 and $CHCl_3$, such as O151⋯H146–C145 (2.60 Å), C150⋯Cl149 (3.21 Å) and C150⋯Cl147 (3.21 Å). In Fig. 3f, the π–π interaction distance between CO_2 and the benzene ring is 3.10 Å, which is almost equivalent to the parameter in Fig. S1a.† When $CHCl_3$ lies in the cage, only the C–H in COM-e forms a hydrogen bond with CO_2 and C–H⋯π interaction with the benzene ring. Hence, the C–H bond length in this structure is the largest (1.089 Å) according to Table 1. In a word, the more forces are, the greater the molecule will change. As expected, the change in the bond length and bond angle of CO_2 in COM-e should be the largest.

Table 1 Interaction energy in different conformations and structural parameters of the molecules (unit: kcal mol^{-1})

Complex	Interaction energy (E_{abs})	CO_2			$CHCl_3$
		Bond angle (°)	Bond length (Å)		
CO_2		180	1.163		
C–H					1.086
Cage $3^0 13^6$					
COM-a	−9.2	179.711	1.161	1.167	1.085
COM-b	−15.9	179.817	1.161	1.166	1.092
COM-c	−12.6	179.736	1.161	1.167	1.085
COM-d	−18.2	179.782	1.164	1.162	1.086
COM-e	−19.0	178.569	1.165	1.162	1.089
COM-f	−19.4	178.848	1.165	1.162	1.085
Cage $3^6 13^0$					
ABS-a	−9.7	179.872	1.166	1.162	1.085
ABS-b	−16.0	178.621	1.164	1.163	1.086
ABS-c	−12.7	179.798	1.164	1.163	1.087
ABS-d	−17.0	179.833	1.163	1.163	1.088
ABS-e	−22.9	176.277	1.160	1.167	1.089
ABS-f	−19.5	178.828	1.165	1.162	1.089
Cage $3^3 13^3$					
SYS-a	−10.3	179.672	1.160	1.167	1.086
SYS-b	−16.2	179.669	1.160	1.167	1.086
SYS-c	−14.3	179.637	1.162	1.166	1.085
SYS-d	−18.1	179.835	1.163	1.163	1.088
SYS-e	−23.6	179.242	1.162	1.165	1.086
SYS-f	−20.7	178.887	1.162	1.166	1.087

Cage $3^6 13^0$. In the same way, after replacing the six vertices of the cage, six conformations were still investigated in Fig. 4. When CO_2 is in the cage (Fig. 4a–c), it only interacts with a benzene ring, which is different from $3^0 13^6$. In Fig. 4a (ABS-a), the distance between CO_2 and the benzene ring (3.09 Å) is smaller than that in COM-a, and there remains a hydrogen bond with the benzene ring O176⋯H21–C21 (2.69 Å). Similarly, in Fig. 4b, although the $CHCl_3$ at the window in ABS-b has only one hydrogen bond with the cage, there are two hydrogen bonds between CO_2 and the cavity window. Moreover, the π–π interaction distance is smaller than that in COM-b. When $CHCl_3$ stands on the surface in ABS-c (Fig. 4c), between the Cl atom and the benzene ring is Cl172⋯π interaction, of which the distance (3.28 Å) is smaller than that in COM-c (3.36 Å).

The positions of $CHCl_3$ in the cage are almost indistinguishable after exchanging the molecules in the cavity of POC (Fig. 4d–f). It can be seen that the three chlorine atoms in chloroform all face three windows. From the perspective of interaction distance, the distance of C–H⋯π is greater than that in Cage $3^0 13^6$. But in Fig. 4d (ABS-d), compared with COM-d in Fig. 3d, $CHCl_3$ has two more hydrogen bonds with the cage. In Fig. 4e, in ABS-e are three hydrogen bonds. It is noteworthy that one of them is the hydrogen bond between CO_2 and $CHCl_3$. In Fig. 4f (ABS-f), the possible interaction is the π–π interaction (3.07 Å) which is smaller than that in COM-f (3.10 Å). According to Table 1, the existence of C–H⋯π causes the C–H bond length to become longer. In ABS-e, the reason why the bond length and bond angle in CO_2 changes drastically is that there remain atoms interacting with it.

Cage $3^3 13^3$. From the perspective of the structure of the cage, the former two structures have a higher degree of symmetry. In order to increase the disorder of the cage, the vertices were replaced with "**3**" and "**13**" to obtain the cage $3^3 13^3$ in Fig. 5. When CO_2 lies in the cage (Fig. 5a–c), there is always a strong π–π interaction between CO_2 and the benzene ring, which is stronger than the similar corresponding structures in Cage $3^0 13^6$ and Cage $3^6 13^0$. In Fig. 5b, compared with COM-b and ABS-b, in terms of numbers, the chloroform in SYS-b has maximum number of hydrogen bonds with the cage. In addition, the chloroform in Fig. 4c is not much different from that in ABS-c.

After $CHCl_3$ is placed in the cage, it can be observed that the chlorine and H atoms of $CHCl_3$ in Fig. 5d and e face four windows respectively. Although the interaction of C–H⋯π is relatively weak, there exist a few Cl⋯π interactions in this system, which are not drawn here. More details are described in the reduced density gradient analysis section. It is precisely because of these Cl⋯π actions that $CHCl_3$ is more stable inside the cage. Similarly, the CO_2 at the vertex in Fig. 5d has no hydrogen bond. In Fig. 5e, there are both electrostatic interaction and hydrogen bonding between CO_2 and the cage, of which O163⋯H158–C162 (2.19 Å) seems stronger. In Fig. 5f, CO_2 interacts with both the surface and the vertex.

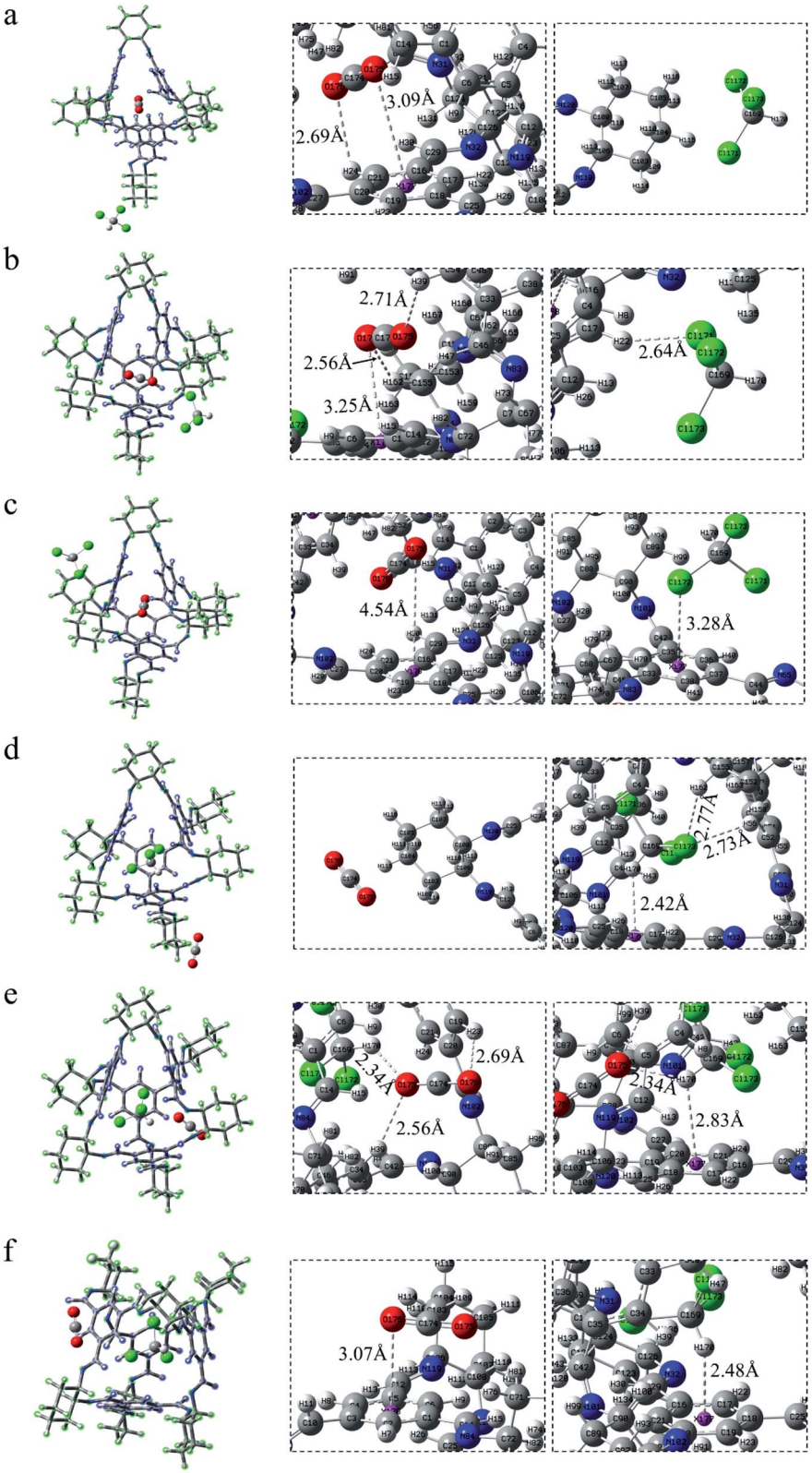

Fig. 4 CO_2 lies in the cage $3^6 13^0$ whereas $CHCl_3$ stands (a) ABS-a, at the vertex; (b) ABS-b, inside the window; (c) ABS-c, on the surface. $CHCl_3$ lies in the cavity $3^0 13^6$ whereas CO_2 stands (d) ABS-d, at the vertex; (e) ABS-e, inside the window; (f) ABS-f, on the surface.

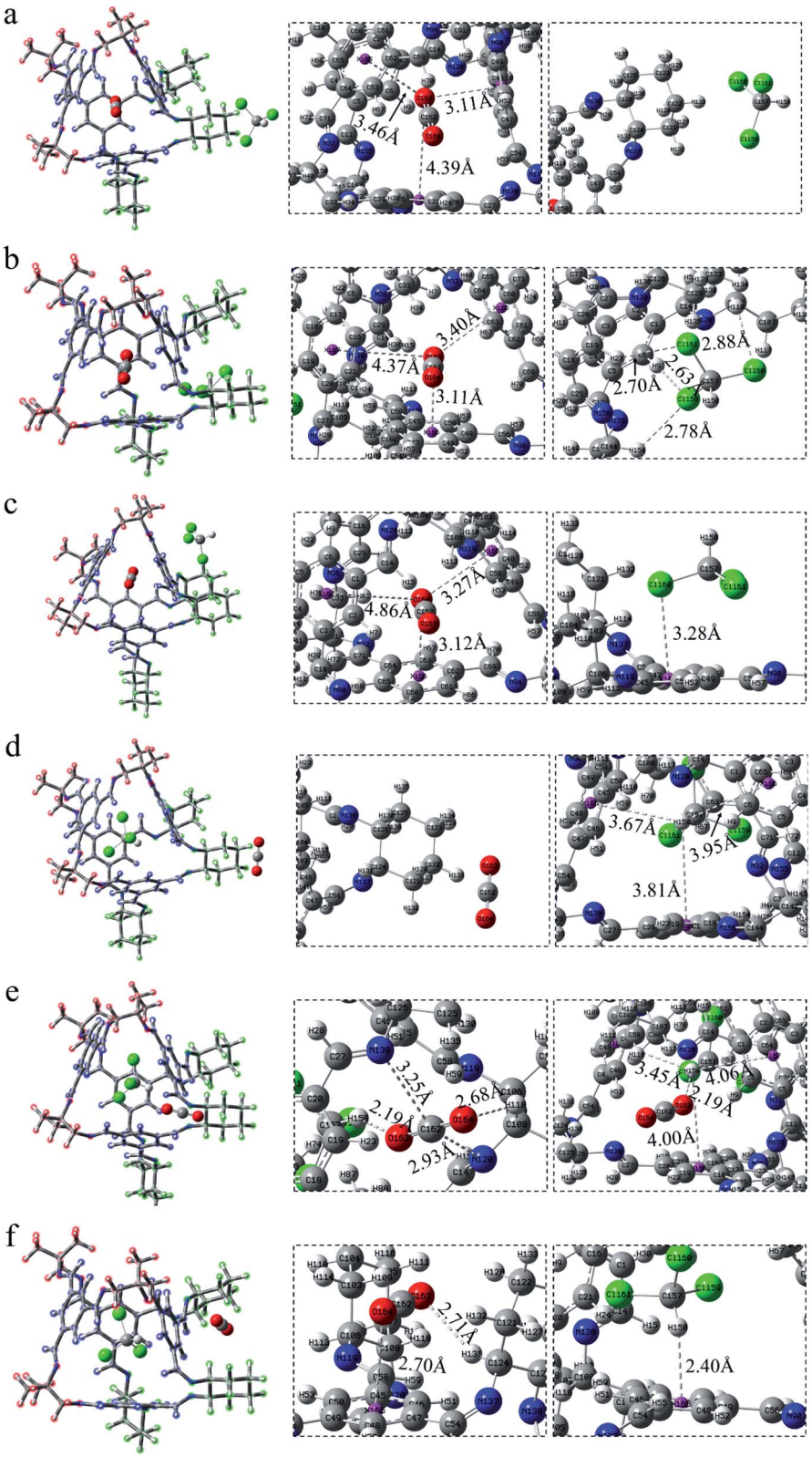

Fig. 5 CO_2 lies in the cage $3^3 13^3$ whereas $CHCl_3$ lies (a) SYS-a, at the vertex; (b) SYS-b, inside the window; (c) SYS-c, on the surface. $CHCl_3$ lies in the cavity $3^0 13^6$ whereas CO_2 stands (d) SYS-d, at the vertex; (e) SYS-e, inside the window; (f) SYS-f, on the surface.

In a word, what can be seen from the structural analysis is that carbon dioxide can be steady absorbed in the cages. However, chloroform lies in the cage more stable than carbon dioxide. What's more, different cages have different types of force. Due to the increased structural disorder, the interaction of the formed asymmetric cage ($\mathbf{3^3 13^3}$) seems to be stronger than that of the cage made of a single diamine ($\mathbf{3^0 13^6}$, $\mathbf{3^6 13^0}$).

3.2 Energetics

Comparison on E_{abs} of various conformations. Although the interaction between molecules can be used as a rough criterion for judging the intermolecular distance, it is difficult to compare among different types. Hence, the calculation of the interaction energy is particularly crucial. According to the calculation formula given in the model section, the interaction energies of the above structures were obtained. For a better explanation, here is the absolute value of the interaction energy for comparison. It can be found from Table 1 that on the whole, the interaction energy of chloroform in the cage is greater than that of CO_2 in the cage, which indicates that CO_2 can be separated by $CHCl_3$. In the structural analysis, the molecules at the vertex have weaker force with the cage, and the interaction energy is also the weakest, such as COM-a (-9.2 kcal mol^{-1}) and COM-d (-18.2 kcal mol^{-1}). When CO_2 lies in the cage, the strongest energy is COM-b (-15.9 kcal mol^{-1}) where $CHCl_3$ stands at the window. When $CHCl_3$ is located in the cage, because the type of forces in COM-e is the abundant, its interaction energy is stronger (-19.0 kcal mol^{-1}). It is the much smaller π–π interaction distance in COM-f that results in the strongest energy (-19.4 kcal mol^{-1}). For cage $\mathbf{3^6 13^0}$, according to the data in Table 1, the interaction of chloroform in the cavity is also greater than that of carbon dioxide in the cage. As is shown, the structure ABS-a (-9.7 kcal mol^{-1}) and ABS-d (-17.0 kcal mol^{-1}), which are still situated at the vertex, have the weakest interaction energy. Combined with the previous structural analysis, ABS-b and ABS-e have abundant interactions, leading to the strongest interaction energy which is different from $\mathbf{3^0 13^6}$. As expected, as shown in Table 1, in cage $\mathbf{3^3 13^3}$, the interaction energy between SYS-a and SYS-d is the weakest. In order to gain insight into the stability of the structure more intuitively, we calculated the exchange energy in Table 2. The results calculated are all negative values, which are respectively -3.5, -6.9 and -7.4 kcal mol^{-1}, indicating that chloroform is much more stable in the cage. As the cage changes, this stability gap seems to become larger. It is demonstrated that $CHCl_3$ can replace CO_2 to achieve the purpose of separation.

Table 2 Exchange energy between CO_2 and $CHCl_3$ (unit: kcal mol^{-1})

Complex	Interaction energy (ΔE_{abs})	Exchange energy (ΔE_{exc})
COM-b	−15.9	−3.5
COM-f	−19.4	
ABS-b	−16.0	−6.9
ABS-e	−22.9	
SYS-b	−16.2	−7.4
SYS-e	−23.6	

Table 3 Interaction energy between single molecule and cages (unit: kcal mol^{-1})

Complex	Interaction energy (ΔE_{abs})
COM–CO_2	−6.7
COM–$CHCl_3$	−17.7
ABS–CO_2	−7.1
ABS–$CHCl_3$	−15.2
SYS–CO_2	−7.2
SYS–$CHCl_3$	−16.9

For investigating the force between a single molecule and the cage more simply, six structures were made with carbon dioxide or chloroform in the cage. In Table 3, COM, ABS and SYS represent cage $\mathbf{3^0 13^6}$, $\mathbf{3^6 13^0}$, and $\mathbf{3^3 13^3}$ respectively. The suffix indicates the single molecule in the cage. It can be observed that the interaction energy of CO_2 in the cavity is much smaller than that of $CHCl_3$. Moreover, the cavity of cage $\mathbf{3^3 13^3}$ has the largest interaction energy for CO_2 (-7.2 kcal mol^{-1}), possessing the best adsorption capacity. In addition, the interaction between the three cages and chloroform is relatively strong.

In summary, the interaction energy of chloroform in the cage is larger, indicating that $CHCl_3$ tends to enter the cavity more than CO_2, and consequently, $CHCl_3$ can indeed substitute CO_2. Additionally, the interaction energy at the vertex is the smallest while the energy at the window is the largest. According to Table 1, the interaction energy generally increases with the replacement of vertices. As a matter of fact, the cages prepared from a single diamine (like $\mathbf{3^0 13^6}$, $\mathbf{3^6 13^0}$) have a high degree of symmetry than such scrambled ones (such as $\mathbf{3^3 13^3}$). After replacing the different vertices, the disorder of the system is increased. The interaction energy of the same sites increased because of Cage $\mathbf{3^3 13^3}$ with structural disorder, indicating that it is beneficial for absorption of CO_2 as the disorder of the cage are increased by changing the vertices of the cages.

Absorption capacity of CO_2 in the cage. From the energy analysis above, it is found that such cages are capable of absorb CO_2. Since POCs can absorb carbon dioxide gas, how much gas can be stored is a question worth studying. Solid POCs have both cavities (intrinsic pores) in each cage and voids (extrinsic pores) between different cages. However, this extrinsic pores in the porous liquid will be greatly lost. Greenaway *et al.*[21] found that porous liquids have a gas affinity similar to related porous organic solids with almost no extrinsic porosity. In view of this, we have tried to explore the absorption capacity of a single porous organic cage, dismissing the extrinsic pores (Table 4). As far as a single gas molecule is concerned, the cage $\mathbf{3^3 13^3}$ has the strongest absorption capacity. As the gas concentration increases, the absorption capacity in different cages changes accordingly. For the cage $\mathbf{3^0 13^6}$, when the number of CO_2 is from 1 to 4, the absorption capacity continues to increase. But it begins to decrease when the number adds up to 5. For the cage

Table 4 Interaction energy of each CO_2. (unit: kcal mol^{-1}). The number indicates the equivalent of CO_2

Complex	Interaction energy ($\Delta\bar{E}_{aver}$)
Cage $3^0 13^6$	
CAP–COM-1	−6.7
CAP–COM-2	−6.9
CAP–COM-3	−7.1
CAP–COM-4	−9.8
CAP–COM-5	−7.4
Cage $3^6 13^0$	
CAP–ABS-1	−7.1
CAP–ABS-2	−7.4
CAP–ABS-3	−5.3
CAP–ABS-4	−5.4
CAP–ABS-5	−5.2
Cage $3^3 13^3$	
CAP–SYS-1	−7.2
CAP–SYS-2	−7.4
CAP–SYS-3	−7.1
CAP–SYS-4	−9.5
CAP–SYS-5	−6.3

$3^6 13^0$, at 3 eq., the absorption capacity began to decline significantly. It can be observed that the cavity optimal capacity of this kind of cage is 2 eq. In Fig. 6d, it is worth noting that when there are 5 eq. of CO_2, one of the gas molecules has already overflowed the cavity. The interaction energy trend of the last cage $3^3 13^3$ is similar to that of $3^0 13^6$, which also increases first and then decreases. Briefly, the best absorption conformations of the three cages are drawn in Fig. 6, which are CAP–COM-4 (4 eq.), CAP–ABS-2 (2 eq.), CAP–SYS-4 (4 eq.). As shown in Fig. 6, CO_2 in the cage interacts with both the cavity wall and neighboring carbon dioxide. Especially in Fig. 6b, one of the O atoms of carbon dioxide points to the C atoms from the other one. This force comes from electrostatic interaction. The CO_2 in Fig. 6a and c meets the above arrangement as well. As the concentration of CO_2 increases, the cavity volume of the cage is constantly changing, resulting in the diverse ability to absorb CO_2. When the CO_2 concentration is low (<3 eq.), $3^3 13^3$ stands out, and when the CO_2 concentration is high (≥3 eq.), the absorption capacity of $3^0 13^6$ is strong. In fact, the scrambled cage $3^3 13^3$ is not inferior to the $3^0 13^6$ made of a single diamine in its ability to absorb gas. However, in the sterically hindered solvent PCP, the solubility of cage $3^3 13^3$ (234–242 mg ml^{-1}) is much greater than that of cage $3^0 13^6$ (80 mg ml^{-1}).[17] The increase in solubility can be attributed to the decrease in lattice energy, because these scrambled cages show a greatly reduced tendency to crystallize.[21] To sum up, it is the porous liquid of cage $3^3 13^3$ that has the strongest gas absorbing ability among the three kinds of cages. In addition, for a porous liquid with a high gas absorption capacity, the porous material itself needs to have good adsorption performance and at the same time have a large solubility in the sterically hindered solvent.

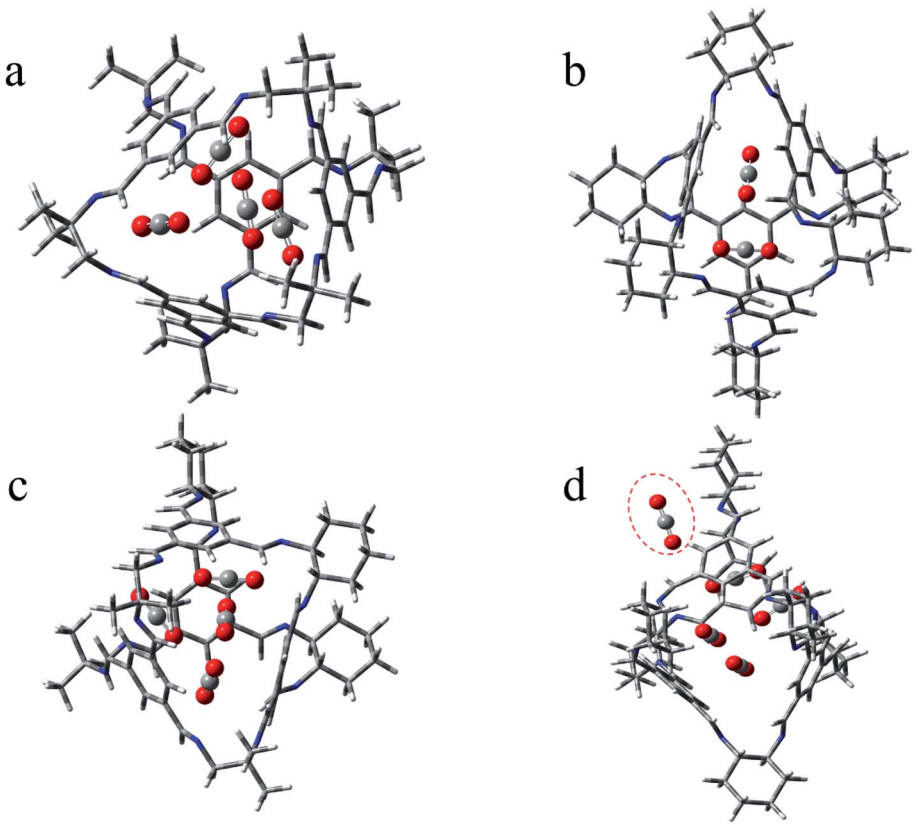

Fig. 6 Optimized configurations for POCs containing CO_2. (a) CAP–COM-4; (b) CAP–ABS-2; (c) CAP–SYS-4; (d) CAP–ABS-5.

3.3 Analysis on the interaction nature of gas absorption

Electrostatic potential analysis. As an important analysis method, electrostatic potential analysis is widely used in non-covalent systems.[27,28,31] The previous structural analysis shows that there exist hydrogen bonding, π–π and C–H···π interactions in the system. It is well known that hydrogen bonds are caused to some extent by electrostatic forces. According to the electrostatic potential analysis, the configuration of the system and the distribution of electron density can be qualitatively understood. As shown in Fig. 7, a series of electrostatic potential surface maps has been drawn. Following the advice of Bader *et al.*,[34] we take the isosurface as 0.001 a.u. In fact, there will always be some electron-deficient and electron-rich regions in the molecule. From bottom to top, the color changes from red to blue. Among them, blue represents a positive surface electrostatic potential, and red is a negative surface electrostatic potential. Although the vertex of the cage is constantly changing, the electronegative area is still concentrated in the center of the benzene ring on the four faces, and the electropositive area is concentrated at the window, that is, the H atom at the edge of the benzene ring. It is worth noting that the end of the chlorine atom along the C–Cl direction in chloroform (Fig. 7a) is blue, indicating that the ESP value in this region is positive. Fig. S1c† shows that there is a certain interaction between the Cl atom and the red benzene ring. Obviously, this interaction is driven by electrostatic force.[35] Related literature shows that this force is called a halogen bond.[36,37] In addition, Politzer *et al.*[35,38,39] found through theoretical calculations that the halogen atoms that form the halogen bond have a positive surface electrostatic potential in the outermost region centered on the R–X axis, which is called σ-hole. As we all know, chlorine atoms and hydrogen atoms form hydrogen bonds. In 2010, Zenaida *et al.*[40] classified halogen bonds and hydrogen bonds as a subset of σ-hole bonding. In chloroform, although the Cl atom has electropositive area on the surface, it is still far less than the positively charged area of H atoms. Generally speaking, the more positive the electrostatic potential, the stronger the force formed, which is consistent with the data in Fig. S1.† In addition, in the CO_2 molecule, since the electronegativity of the O atom is greater than that of the C atom, the electron density near the O atom is greater than the electron density near the C atom. Combined with the structure of the cage, there are a lot of hydrogen atoms in the window. The O atoms in the negatively charged region of CO_2 tend to form hydrogen bonds with the H atoms in the positively charged region of the window. The above proves once again that when CO_2 is located at the window, the interaction becomes stronger.

Reduced density gradient analysis. A reduced density analysis method has been widely used since Yang *et al.*[41] proposed it. In order to determine whether there is a weak interaction in the system, Multiwfn[42] program was first used to plot the relationship between the electron density ρ and the reduced density gradient (RDG). In fact, in the areas of covalent bonding and non-covalent interaction, the value of RDG is very small. As shown in Fig. 8a, there is a spike on the left (<0.025), which is the non-covalent interaction region, while the right (>0.25) represents the covalent bonding region. To distinguish the various types of non-covalent interactions, drawn the relationship between $\sin(\lambda_2)\rho$ and RDG was drawn. Among them, λ_2 is the eigenvalue of the second derivative of the Hessian matrix.[41] The interaction between bonding (<0) and non-bonding (>0) can be distinguished by the sign of λ_2. From bottom to top, the color changes from red to green, and finally to blue. The red area represents strong attraction (such as hydrogen bonding), green indicates van der Waals (like π–π interaction), and blue represents strong mutual repulsion (*e.g.* steric hindrance).

As depicted in Fig. 8b, in COM-f, $CHCl_3$ lies in the cavity and CO_2 is in the surface. What can be seen is that there is indeed C–

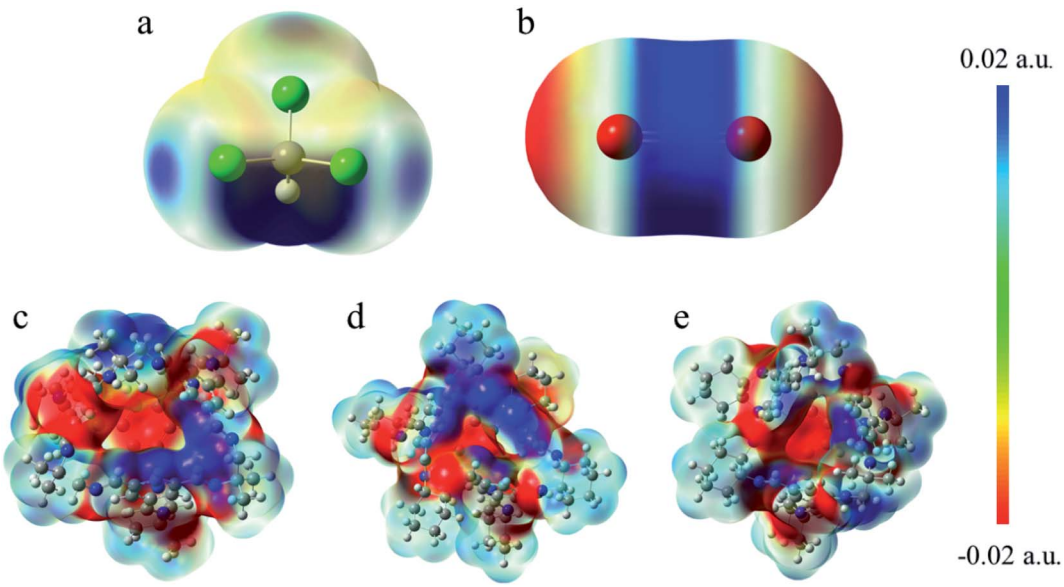

Fig. 7 Electrostatic potential surface mapped on electron total density with an isovalue of 0.001. The colors range from −0.02 a.u. in red to 0.02 a.u. in blue for all the molecules. (a) $CHCl_3$ (b) CO_2 (c) Cage $3^0 13^6$ (d) Cage $3^6 13^0$ (e) Cage $3^3 13^3$.

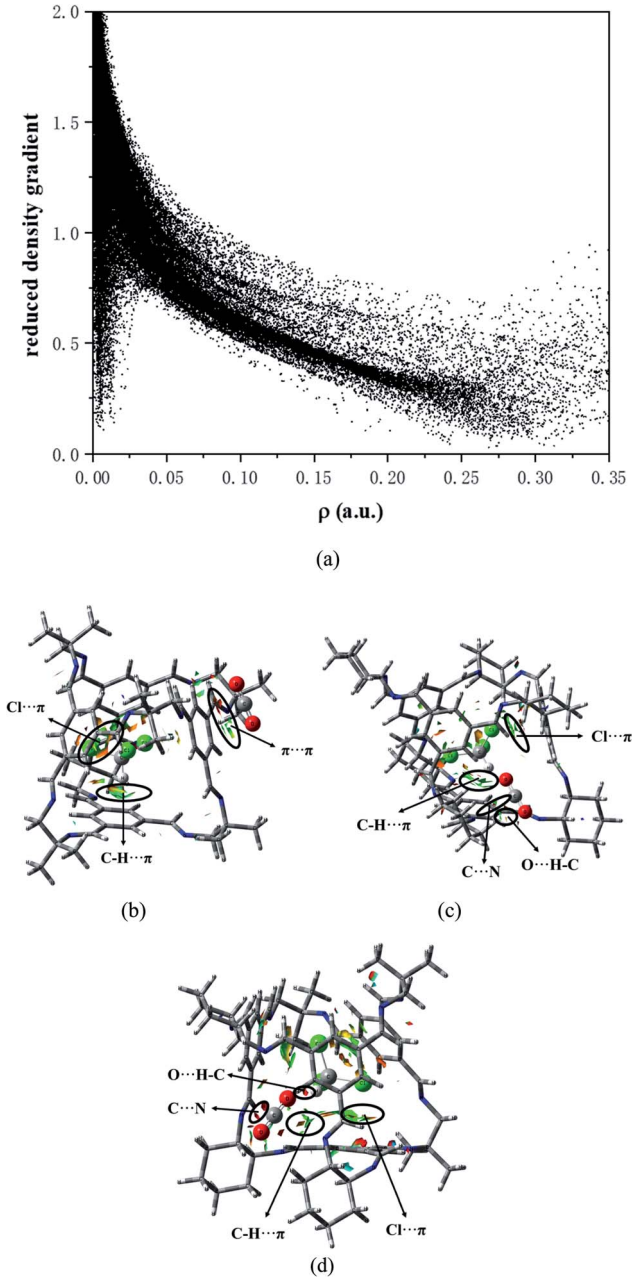

Fig. 8 (a) Plots of the electron density and its reduced density gradient (SYS-e). Gradient isosurfaces ($s = 0.35$ a.u.) for (b) COM-f. (c) ABS-e. (d) SYS-e. The surfaces are colored on a red-green-blue scale according to values of $\sin(\lambda_2)\rho$, ranging from -0.01 to 0.02 a.u. Red indicates strong attractive interactions, and blue indicates strong nonbonded overlap.

H···π between the C–H and benzene ring in chloroform. The area corresponding to the interaction has both red and green, indicating that the interaction has a certain bonding effect. In addition, there remains a π–π interaction between the C=O double bond and the benzene ring. However, it is found that there is a red segment between the C in CO_2 and the benzene ring. This is because the Mulliken charge of C in CO_2 is positive, while the Mulliken charge of C on the benzene ring is positive. Therefore, there is a certain electrostatic effect between the two. Besides, there is a Cl···π interaction between the Cl atom and the benzene ring. Although C–Cl points to the window, between Cl and the benzene ring is a halogen bond. In Fig. 8c, on the one hand, there exists a strong electrostatic interaction between CO_2 at the window and N atoms at the edge. The green segment at the window is a weaker hydrogen bond. On the other hand, there are C–H···π interactions and Cl···π interactions between $CHCl_3$ in the cage and the cavity. Fig. 8d is the RDG diagram of SYS-e. It can be observed that carbon dioxide not only has a strong hydrogen bond with chloroform, but also has a hydrogen bond with the window, which is consistent with the previous structural analysis. Furthermore, C···N electrostatic interaction, C–H···π action and Cl···π action also exist in this structure. In short, RDG analysis shows that when $CHCl_3$ is in the cage, there are C–H···π and Cl···π interactions between the chloroform and the cavity. When CO_2 is located at the window, more atoms interact with it, which proves that the site has a stronger interaction.

4. Conclusion

This work explores the mechanism of carbon dioxide capture and separation in porous liquids. Based on the analysis of structure, energy, ESP and RDG analysis, the following conclusions are drawn:

(1) Structure analysis shows such kind of porous organic cage has a certain absorption capacity for CO_2 through π–π interaction. Compared with CO_2, chloroform is more stable inside the cage due to stronger C–H···π interactions and Cl···π interactions.

(2) In the energy analysis section, the conformations where chloroform lies inside the cage whereas CO_2 stand outside the cage have the strongest interaction energy ranging from -17.0 to -23.6 kcal mol^{-1}. Also, their exchange energy is negative, indicating that chloroform can displace carbon dioxide in the cage and eventually separate it. Combined with the interaction energy of single molecules, it is found that the scrambled cage $\mathbf{3}^3\mathbf{13}^3$ possesses the strongest energy. As far as a single cage is concerned, the optimal CO_2 absorption capacity of the cage $\mathbf{3}^0\mathbf{13}^6$ and the cage $\mathbf{3}^3\mathbf{13}^3$ is 4 eq. while the cage $\mathbf{3}^6\mathbf{13}^0$ is 2 eq.

(3) The electrostatic potential analysis shows that when CO_2 is located at the window, the interaction force is stronger. This is because the O atoms in the negatively charged region of CO_2 tend to form hydrogen bonds with the H atoms in the positively charged region of the window.

(4) The RDG analysis shows that there exists weak interaction in the system. Furthermore, it is confirmed again that there are C–H···π and Cl···π interactions between chloroform and the cavity.

Conflicts of interest

The authors declared that they have no conflicts of interest to this work.

Acknowledgements

This work was financially supported by the National Natural Science Foundation of China (No. 21808092, 21878133,

22078135), China Postdoctoral Science Foundation (2019M651742), the Science and Technology project of Southwest Guizhou Autonomous Prefecture (2019-2-51), and the Youth growth project of GuiZhou Provincial Educational Department (KY[2019]220). This research work is supported by the high performance computing platform of Jiangsu University.

References

1 Q. Wang and D. Astruc, *Chem. Rev.*, 2020, **120**, 1438–1511.
2 J. Yu, L. H. Xie, J. R. Li, Y. Ma, J. M. Seminario and P. B. Balbuena, *Chem. Rev.*, 2017, **117**, 9674–9754.
3 A. Torrisi, R. G. Bell and C. Mellot-Draznieks, *Cryst. Growth Des.*, 2010, **10**, 2839–2841.
4 A. Samanta, A. Zhao, G. K. H. Shimizu, P. Sarkar and R. Gupta, *Ind. Eng. Chem. Res.*, 2011, **51**, 1438–1463.
5 J. G. Min, K. C. Kemp, H. Lee and S. B. Hong, *J. Phys. Chem. C*, 2018, **122**, 28815–28824.
6 W. Jeong and J. Kim, *J. Phys. Chem. C*, 2016, **120**, 23500–23510.
7 S. Zeng, X. Zhang, L. Bai, X. Zhang, H. Wang, J. Wang, D. Bao, M. Li, X. Liu and S. Zhang, *Chem. Rev.*, 2017, **117**, 9625–9673.
8 M. Pan and C. Wang, *ACS Symp. Ser.*, 2015, **1194**, 341–369.
9 J. F. Brennecke and B. E. Gurkan, *J. Phys. Chem. Lett.*, 2010, **1**, 3459–3464.
10 M. Ramdin, T. W. de Loos and T. J. H. Vlugt, *Ind. Eng. Chem. Res.*, 2012, **51**, 8149–8177.
11 H. Liu, J. Huang and P. Pendleton, *ACS Symp. Ser.*, 2012, **1097**, 153–175.
12 J. Wang, Z. Song, H.-Y. Cheng, L. Chen, L. Deng and Z. Qi, *ACS Sustainable Chem. Eng.*, 2018, **6**, 12025–12035.
13 N. O'Reilly, N. Giri and S. L. James, *Chem.–Eur. J.*, 2007, **13**, 3020–3025.
14 J. Zhang, S. H. Chai, Z. A. Qiao, S. M. Mahurin, J. Chen, Y. Fang, S. Wan, K. Nelson, P. Zhang and S. Dai, *Angew. Chem., Int. Ed.*, 2015, **54**, 932–936.
15 K. Jie, N. Onishi, J. A. Schott, I. Popovs, D. E. Jiang, S. Mahurin and S. Dai, *Angew. Chem., Int. Ed.*, 2020, **59**, 2268–2272.
16 L. Ma, C. J. E. Haynes, A. B. Grommet, A. Walczak, C. C. Parkins, C. M. Doherty, L. Longley, A. Tron, A. R. Stefankiewicz, T. D. Bennett and J. R. Nitschke, *Nat. Chem.*, 2020, **12**, 270–275.
17 N. Giri, M. G. Del Pópolo, G. Melaugh, R. L. Greenaway, K. Rätzke, T. Koschine, L. Pison, M. F. C. Gomes, A. I. Cooper and S. L. James, *Nature*, 2015, **527**, 216–220.
18 M. Costa Gomes, L. Pison, C. Cervinka and A. Padua, *Angew. Chem., Int. Ed.*, 2018, **57**, 11909–11912.
19 J. Cahir, M. Y. Tsang, B. Lai, D. Hughes, M. A. Alam, J. Jacquemin, D. Rooney and S. L. James, *Chem. Sci.*, 2020, **11**, 2077–2084.
20 W. Shan, P. F. Fulvio, L. Kong, J. A. Schott, C. L. Do-Thanh, T. Tian, X. Hu, S. M. Mahurin, H. Xing and S. Dai, *ACS Appl. Mater. Interfaces*, 2018, **10**, 32–36.
21 R. L. Greenaway, D. Holden, E. G. B. Eden, A. Stephenson, C. W. Yong, M. J. Bennison, T. Hasell, M. E. Briggs, S. L. James and A. I. Cooper, *Chem. Sci.*, 2017, **8**, 2640–2651.
22 N. Giri, C. E. Davidson, G. Melaugh, M. G. Del Pópolo, J. T. A. Jones, T. Hasell, A. I. Cooper, P. N. Horton, M. B. Hursthouse and S. L. James, *Chem. Sci.*, 2012, **3**, 2153.
23 R. J. Kearsey, B. M. Alston, M. E. Briggs, R. L. Greenaway and A. I. Cooper, *Chem. Sci.*, 2019, **10**, 9454–9465.
24 G. Melaugh, N. Giri, C. E. Davidson, S. L. James and M. G. Del Pópolo, *Phys. Chem. Chem. Phys.*, 2014, **16**, 9422–9431.
25 T. Tozawa, J. T. Jones, S. I. Swamy, S. Jiang, D. J. Adams, S. Shakespeare, R. Clowes, D. Bradshaw, T. Hasell, S. Y. Chong, C. Tang, S. Thompson, J. Parker, A. Trewin, J. Bacsa, A. M. Slawin, A. Steiner and A. I. Cooper, *Nat. Mater.*, 2009, **8**, 973–978.
26 F. Zhang, F. Yang, J. Huang, B. G. Sumpter and R. Qiao, *J. Phys. Chem. B*, 2016, **120**, 7195–7200.
27 H. Li, Y. Chang, W. Zhu and C. Wang, *Phys. Chem. Chem. Phys.*, 2015, **17**, 28729–28742.
28 H. Li, Y. Chang, W. Zhu, W. Jiang, M. Zhang, J. Xia, S. Yin and H. Li, *J. Phys. Chem. B*, 2015, **119**, 5995–6009.
29 J. Zhang, N. Lv, Y. Chao, L. Chen, W. Fu, J. Yin, H. Li, W. Zhu and H. Li, *J. Mol. Graphics Modell.*, 2020, **100**, 107694.
30 K. D. Vogiatzis, W. Klopper and J. Friedrich, *J. Chem. Theory Comput.*, 2015, **11**, 1574–1584.
31 H. Li, B. Zhang, W. Jiang, W. Zhu, M. Zhang, C. Wang, J. Pang and H. Li, *Green Energy Environ.*, 2019, **4**, 38–48.
32 W. Jiang, H. Jia, H. Li, L. Zhu, R. Tao, W. Zhu, H. Li and S. Dai, *Green Chem.*, 2019, **21**, 3074–3080.
33 M. J. Frisch, G. W. Trucks, H. B. Schlegel, G. E. Scuseria, M. A. Robb, J. R. Cheeseman, *et al.*, *Gaussian 16*, Gaussian, Inc., Wallingford, CT, USA, 2016.
34 R. F. W. Bader, M. T. Carroll, J. R. Cheeseman and C. Chang, *J. Am. Chem. Soc.*, 1987, **109**, 7968–7979.
35 P. Politzer, J. S. Murray and T. Clark, *Phys. Chem. Chem. Phys.*, 2010, **12**, 7748–7757.
36 G. Cavallo, P. Metrangolo, R. Milani, T. Pilati, A. Priimagi, G. Resnati and G. Terraneo, *Chem. Rev.*, 2016, **116**, 2478–2601.
37 H. Wang, W. Wang and W. J. Jin, *Chem. Rev.*, 2016, **116**, 5072–5104.
38 P. Politzer, J. S. Murray and T. Clark, *Phys. Chem. Chem. Phys.*, 2013, **15**, 11178–11189.
39 J. S. Murray, P. Lane, T. Clark, K. E. Riley and P. Politzer, *J. Mol. Model.*, 2012, **18**, 541–548.
40 Z. P. Shields, J. S. Murray and P. Politzer, *Int. J. Quantum Chem.*, 2010, **110**, 2823–2832.
41 E. R. Johnson, S. Keinan, P. Mori-Sánchez, J. Contreras-García, A. J. Cohen and W. Yang, *J. Am. Chem. Soc.*, 2010, **132**, 6498–6506.
42 T. Lu and F. Chen, *J. Comput. Chem.*, 2012, **33**, 580–592.